

# Probing nuclear skins and halos with elastic electron scattering

C.A. Bertulani\*

*Department of Physics, University of Arizona, Tucson, AZ 85721, USA*

(Dated: February 9, 2020)

## Abstract

We investigate the elastic electron scattering off nuclei far from the stability line. The effects of the neutron and proton skins and halos on the differential cross sections are explored. Examples are given for the charge distribution in Sn isotopes and its relation to the neutron skin. The neutron halo in  $^{11}\text{Li}$  and the proton halo in  $^8\text{B}$  are also investigated. Particular interest is paid to the inverse scattering problem and its dependence on the experimental accuracy. These studies are of particular interest for the upcoming electron ion colliders at the GSI and RIKEN facilities.

PACS numbers: 25.30.Bf, 21.10.Ft, 25.60.-t

Keywords: Electron scattering, charge distribution, unstable nuclear beams.

arXiv:nucl-th/0604044v1 19 Apr 2006

---

\*Electronic address: bertulani@physics.arizona.edu

## I. INTRODUCTION

The use of radioactive nuclear beams produced by fragmentation in high-energy heavy-ion reactions lead to the discovery of halo nuclei, such as  ${}^{11}\text{Li}$ , about 20 years ago [1]. Nowadays a huge number of  $\beta$ -unstable nuclei far from stability are being studied thanks to further technical improvements. Unstable nuclei far from stability are known to play an important role in nucleosynthesis. Detailed studies of the structure and their reactions will have unprecedented impact on astrophysics [2].

The first experiments with unstable nuclear beams aimed at determining nuclear sizes by measuring the interaction cross section in high energy collisions [1]. Successive use of this technique has yielded nuclear size data over a wide range of isotopes. Other techniques, e.g. isotope-shift measurements, have allowed to extract the charge size. The growth of a neutron skin with the neutron number in several isotopes have been deduced from nuclear- and charge-size data [3].

The charge (nucleon) density distribution can also be determined by electron (hadron) scattering experiments. Among hadron scattering, proton elastic scattering at intermediate energies is a good tool to probe the nucleon density distributions, due to its larger mean-free path in the nuclear medium. But, undoubtedly, it is the electron scattering off nuclei that provides the most direct information about charge distribution, which is closely related to the spatial distribution of protons [4].

A technical proposal for an electron-heavy-ion collider has been incorporated in the GSI/Germany physics program [5]. A similar program exists for the RIKEN/Japan facility [6]. In both cases the main purpose is to study the structure of nuclei far from the stability line. The advantages of using electrons in the investigation of the nuclear structure are mainly related to the fact that the electron-nucleus interaction is relatively weak. For this reason multiple scattering effects are usually neglected and the scattering process is described in terms of perturbation theory. Since the reaction mechanism in perturbation theory is well under control the connection between the cross section and quantities such as charge distributions, transition densities, response functions etc., is well understood [7].

Theoretically, the shape of the density distribution includes detailed information on the internal nuclear structure. In the independent particle shell model the density distribution is the squared sum of the single-particle wave functions. No measurement of either nucleon

distribution or the charge distribution for short-lived radioactive nuclei has been made so far.

Under the impulse approximation, or plane wave Born approximation, the charge form factor can be determined from the differential cross section of elastic electron scattering. Since the charge distribution,  $\rho_{ch}(r)$ , is obtained from the charge form factor by a Fourier transformation, one can experimentally determine  $\rho_{ch}(r)$  by differential cross-section measurements covering a wide range of momentum transfer  $q$ . One can obtain information on the size and diffuseness when the charge form factor is measured at least up to the first maximum. To do this within a reasonable measuring time of one week, a luminosity larger than  $10^{26} \text{ cm}^{-2}\text{s}^{-1}$  is required, for example for the  $^{132}\text{Sn}$  isotope [5].

On the theoretical side the difference between the proton and neutron distributions can be obtained in the framework of Hartree-Fock (HF) method (see for example [8]) or Hartree-Fock-Bogoliubov (HFB) method (see for example [9]). As a rule of thumb, a theoretical calculation of the nuclear density is considered good when it reproduces the data on elastic electron scattering. But some details of the theoretical densities might not be accessible in the experiments, due to poor resolution or limited experimental reach of the momentum transfer  $q$ .

In this work we study the general features of elastic electron scattering off unstable nuclei. A previous assessment of this kind has been done in ref. [10]. Here we focus on using the general features of what is theoretically known about skins and halos to look for their respective signatures in the data. Only a few specific and representative nuclear density cases are used. The paper is organized as follows. After a general introduction of elastic electron scattering in section 2, we show in section 3 how the telltales of neutron and proton skins and halos become visible in the differential cross sections for elastic electron scattering. Section 4 presents a study of the inverse scattering problem, which poses a challenge for extracting the charge density profiles from the experimental data. The conclusions will be presented in section 5. A few useful analytical formulae used in the manuscript are left for the Appendix.

## II. ELASTIC ELECTRON SCATTERING

In the plane wave Born approximation (PWBA) the relation between the charge density and the cross section is given by

$$\left(\frac{d\sigma}{d\Omega}\right)_{\text{PWBA}} = \frac{\sigma_M}{1 + (2E/M_A) \sin^2(\theta/2)} |F_{ch}(q)|^2, \quad (1)$$

where  $\sigma_M = (Z^2\alpha^2/4E^2) \cos^2(\theta/2) \sin^{-4}(\theta/2)$  is the Mott cross section, the term in the denominator is a recoil correction,  $E$  is the electron total energy,  $M_A$  is the mass of the nucleus and  $\theta$  is the scattering angle.

The charge form factor  $F_{ch}(q)$  for a spherical mass distribution is given by

$$F_{ch}(q) = 4\pi \int_0^\infty dr r^2 j_0(qr) \rho_{ch}(r), \quad (2)$$

where  $q = 2k \sin(\theta/2)$  is the momentum transfer,  $k$  is the electron momentum, and  $E = \sqrt{k^2c^2 + m_e^2c^4}$ . The low momentum expansion of eq. 2 yields the leading terms

$$F_{ch}(q) = 1 - \frac{q^2}{6} \langle r_{ch}^2 \rangle + \dots. \quad (3)$$

Thus, a measurement at low momentum transfer yields a direct assessment of the mean square radius of the charge distribution,  $\langle r_c^2 \rangle^{1/2}$ . However, as more details of the charge distribution is probed more terms of this series are needed and, for a precise description of it, the form factor dependence for large momenta  $q$  is needed.

A theoretical calculation of the charge density entering eq. 2 can be obtained in many ways. Let  $\rho_p(\mathbf{r})$  and  $\rho_n(\mathbf{r})$  denote the point distributions of the protons and the neutrons, respectively, as calculated, e.g. from single-particle wavefunctions obtained from an average one-body potential well, the latter in general being different for protons and neutrons. If  $f_{Ep}(\mathbf{r})$  and  $f_{En}(\mathbf{r})$  are the spatial charge distributions of the proton and the neutron in the non-relativistic limit, then the charge distribution of the nucleus is given by

$$\rho_{ch}(\mathbf{r}) = \int \rho_p(\mathbf{r}') f_{Ep}(\mathbf{r} - \mathbf{r}') d^3r' + \int \rho_n(\mathbf{r}') f_{En}(\mathbf{r} - \mathbf{r}') d^3r'. \quad (4)$$

The second term on the right-hand side of eq. 4 plays an important role in the interpretation of the charge distribution of some nuclear isotopes. For example, the half-density charge radius increases 2% from  $^{40}\text{Ca}$  to  $^{48}\text{Ca}$ , whereas the surface thickness decreases by 10% with the result that there is more charge in the surface region of  $^{40}\text{Ca}$  than of  $^{48}\text{Ca}$

[11]. This also results that the rms charge radius of  $^{48}\text{Ca}$  is slightly smaller than that of  $^{40}\text{Ca}$ . The reason for this anomaly is that the added  $f_{7/2}$  neutrons contribute negatively to the charge distribution in the surface and more than compensate for the increase in the rms radius of the proton distribution.

For the proton the charge density  $f_{Ep}(r)$  in eq. 4 is taken as an exponential function, what corresponds to a form factor  $G_{Ep}(q) \equiv \tilde{f}_{Ep}(q) = (1 + q^2/\Lambda^2)^{-1}$ . For the neutron a good parametrization is  $G_{En}(q) = -\mu_n\tau G_{Ep}(q)/(1 + p\tau)$ , where  $\mu_n$  is the neutron magnetic dipole moment and  $\tau = q^2/4m_N$ . We will use  $\Lambda^2 = 0.71 \text{ fm}^{-2}$  (corresponding to a proton rms radius of 0.87 fm) and  $p = 5.6$ , which Galster et al. [12] have shown to reproduce electron-nucleon scattering data.

Eqs. 1-4 are based on the first Born approximation. They give good results for light nuclei (e.g.  $^{12}\text{C}$ ) and high-energy electrons. For large- $Z$  nuclei the agreement with experiments is only of a qualitative nature. The effects of distortion of the electron waves have been studied by many authors (see, e.g. ref. [13, 14]). Following ref. [15], the correction due to Coulomb distortion at forward angles is approximately given by

$$\left(\frac{d\sigma}{d\Omega}\right)_{\text{corrected}} \simeq \left(\frac{d\sigma}{d\Omega}\right)_{\text{PWBA}} \left[1 + \beta \frac{Ze^2}{\hbar c}\right], \quad (5)$$

with

$$\beta = \frac{120}{x^2} \left\{ -\frac{1}{160x^3} \left[ 1 + \frac{3}{2} \cos(2x) + 3x \sin(2x) + \frac{x^2}{3} (4 + 5 \cos(2x)) + \frac{10}{3} x^3 \sin(2x) \right] \right. \\ \left. + \frac{x}{60} \left[ \frac{9}{4} - \cos(2x) \right] + \frac{x^2}{60} [\pi - 2 \text{Si}(2x)] + n_1(2x) \left[ \frac{1}{16x} + \frac{x}{40} \right] \right\}, \quad (6)$$

where  $x = pR_{ch}/\hbar$ ,  $R_{ch}$  is the nuclear charge radius, Si is the sine integral,  $\text{Si}(x) = \int_0^\infty dt \sin t/t$ , and  $n_i(x)$  is the spherical Bessel function of the second kind. Using this formula one finds a correction of less than 0.1% for  $^{12}\text{C}$  and electrons with energy  $E = 1$  GeV. This correction increases to 6% for tin isotopes.

More important than the change in the normalization of the cross section is the displacement of the minima. As shown by Antonov et al. [10] the PWBA equation reproduces the shift of the minima to lower  $q$ 's (due to the Coulomb attraction felt by the electrons) if one replaces the momentum transfer  $q$  in the PWBA formula with the effective momentum transfer  $q_{eff} = [1 + (Z\alpha/R_{ch}E)]$ , where  $E$  is the electron energy.

A realistic description of the elastic electron scattering cross section requires the full solution of the Dirac equation. The Dirac equation for the elastic scattering from a charge

distribution can be found in standard textbooks, e.g. [16]. Numerous DWBA codes based on Dirac distorted waves have been developed and are public. Since the inclusion of Coulomb distortion is straight-forward, we will concentrate on the information which can be extracted from elastic electron scattering, which is encoded in the form-factor of eq. 2. Later we will study the problem of extracting the full nuclear density from the form factor. For simplicity, we will also neglect the effect of the charge distribution of the neutron itself. This effect is particularly important for large  $q$ -transfers [10]. For heavy nuclei it can change  $|F_{ch}(q)|^2$  by 10-20% in the  $q$ -range of 1.5 - 2 fm<sup>-1</sup>.

### III. SKINS AND HALOS

#### A. Neutron Skins

Appreciable differences between neutron and proton radii are expected [17] to characterize the nuclei at the border of the stability line. The liquid drop formula expresses the binding energy of a nucleus with  $N$  neutrons and  $Z$  protons as a sum of bulk, surface, symmetry and Coulomb energies

$$\frac{E}{A} = -a_V A + a_S A^{2/3} + S \frac{(N - Z)^2}{A} + a_C \frac{Z^2}{A^{1/3}}, \quad (7)$$

where  $a_V$ ,  $a_S$ ,  $S$  and  $a_C$  are parameters fitted to the experimental data of binding energy of nuclei.

This equation does not distinguish between surface ( $S$ ) and volume ( $V$ ) symmetry energies. As shown in ref. [18], this can be achieved by partitioning the particle asymmetry as  $N - Z = N_S - Z_S + N_V - Z_V$ . The total symmetry energy  $S$  then takes on the form

$$S = S_V \frac{(N_V - Z_V)^2}{A} + S_S \frac{(N_S - Z_S)^2}{A^{2/3}}. \quad (8)$$

Minimizing under fixed  $N - Z$  leads to an improved liquid drop formula [18] with the term  $S_V(N - Z)^2/A$  replaced by

$$S_V \frac{(N - Z)^2}{A[1 + (S_V/S_S) A^{-1/3}]}. \quad (9)$$

The same approach also yields a relation between the neutron skin  $R_{np} = R_n - R_p$ , and  $S_S$ ,  $S_V$ , namely [18]

$$\frac{R_n - R_p}{R} = \frac{A}{6NZ} (N_S - Z_S) = \frac{A}{6NZ} \frac{N - Z - (a_C/12S_V) Z A^{2/3}}{1 + (S_S/S_V) A^{1/3}}, \quad (10)$$

where  $R = (R_n + R_p)/2$ .

Here the Coulomb contribution is essential; e.g. for  $N = Z$  the neutron skin  $R_{np}$  is negative due to the Coulomb repulsion of the protons. A wide variation of values of  $S_V$  and  $S_S$  can be found in the literature. These values have been obtained by comparing the above predictions for energy and neutron skin to theoretical calculations of nuclear densities and experimental data on other observables [18, 19]. For heavy nuclei, with  $A \gg 1$ ,  $NZ \simeq A^2/2$ , and using  $a_C = 0.69$  MeV,  $S_V = 28$  MeV and  $R = 1.2A^{1/3}$  fm, one gets

$$R_{np} = R_n - R_p \simeq 0.8 \left( \frac{S_V}{S_S} \right) (\delta - 2.05 \times 10^{-3} Z A^{-2/3}) \text{ fm}, \quad (11)$$

where  $\delta = (N - Z)/A$  is the asymmetry parameter. The linear dependence of  $R_{np}$  with  $\delta$  is easy to show. In fact, if one assumes that the central densities for neutrons and protons are roughly the same and that they are both described by a uniform distribution with sharp-cutoff radii,  $R_n$  and  $R_p$ , one finds  $R_{np} \simeq 0.2A^{1/3}\delta$  fm. Of course, the sharp sphere model is much too simplified and considerations of minimization of volume and surface energy dependence lead to the improved formula, eq. 11.

On the experimental front, a study of antiprotonic atoms described in ref [20] obtained the following expression for the neutron skin of stable nuclei in terms of the root mean square (rms) radii of protons and neutrons

$$\Delta r_{np} = \langle r_n^2 \rangle^{1/2} - \langle r_p^2 \rangle^{1/2} = (-0.04 \pm 0.03) + (1.01 \pm 0.15) \delta \text{ fm}. \quad (12)$$

The relation of the mean square radii with the half-density radii is given by  $\langle r_n^2 \rangle = 3R_n^2/5 + 7\pi^2 a_n^2/5$ , where  $a_n$  is the diffuseness parameter. For heavy nuclei, assuming  $a_n = a_p \ll R_n, R_p$ , one gets the same linear dependence on the asymmetry parameter as in eq. 11 if one uses  $S_V/S_S = 1.63$  fm, in agreement with studies described in ref. [19].

In this work we will use eq. 12 as the starting point for accessing the dependence of electron scattering on the neutron skin of heavy nuclei. Extrapolating the above formula for heavy nuclei, and applying it to calcium isotopes as an example, one obtains that the neutron skin varies from  $-0.15$  fm for  $^{35}\text{Ca}$  (proton-rich with negative neutron skin) to  $0.25$  fm for  $^{53}\text{Ca}$ .

For unstable nuclei no study as the one leading to eq. 12 are experimentally available. Nucleon knockout reactions with secondary unstable nuclear beams, and other techniques, have been used to determine the interaction radii of neutron rich nuclei [1]. These radii are

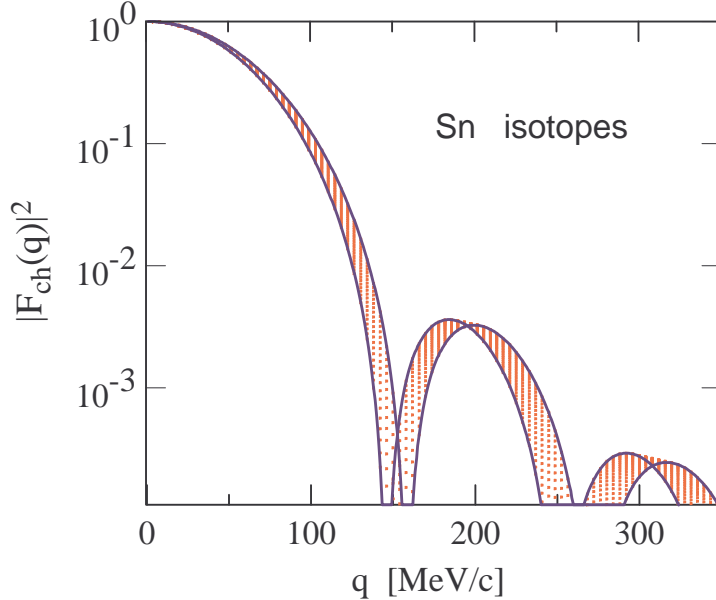


FIG. 1: The (normalized) charge form factor squared for elastic electron scattering off tin isotopes, as a function of the momentum transfer. The two curves are for the extreme values of the asymmetry parameter  $\delta = (N - Z)/A$ . The curves form an envelope around other curves with intermediary values of  $\delta$ .

thought to represent the extension of the neutron distribution in such nuclei. But very little is known about their charge distribution.

For heavy nuclei the charge and neutron distributions can be described by a Fermi distribution with a form factor closely given by expression 37 of the Appendix. The diffuseness is usually much smaller than the half-density radius,  $a_{p,n} \ll R_{p,n}$ . The neutron skin is then given by  $R_{np} = R_n - R_p \simeq \sqrt{5/3} \Delta r_{np}$ . We further assume that the nuclear charge radius in eq. 37 is given by  $R_p = 1.2A^{1/3} \text{ fm} - R_{np}/2$  with  $\Delta r_{np}$  given by eq. 12. Figure 1 shows the (charge normalized to unit) form factor squared for elastic electron scattering off tin isotopes, as a function of the momentum transfer. The two solid curves are for the extreme values of the asymmetry parameter  $\delta = (N - Z)/A$ . The curves form an envelope around other curves with intermediary values of  $\delta$ . The first and second minima of the form factors occur at  $q_1 = 4.49/R_p$  and  $q_2 = 7.73/R_p$ , respectively, corresponding to the solution of the transcendental equation  $\tan(qR_p) = qR_p$ , as becomes evident by inspection of eq. 37.

The linear dependence of  $R_p$  with the neutron skin (and with the asymmetry parameter

$\delta$ ), also imply a linear dependence of the position of the minima,

$$q_1 \simeq \frac{3.74}{A^{1/3}} \left[ 1 - 0.535 \frac{(N - Z)}{A^{4/3}} \right]^{-1} \text{ fm}^{-1}, \quad \text{and} \quad q_2 = 1.72 q_1 . \quad (13)$$

For  $^{100}\text{Sn}$  the first minimum is expected to occur at  $q_1 = 0.806 \text{ fm}^{-1} = 159 \text{ MeV}/c$ , while for  $^{132}\text{Sn}$  it occurs at  $q_1 = 0.754 \text{ fm}^{-1} = 149 \text{ MeV}/c$ .

Figure 2 shows the value of  $q_1$  for elastic electron scattering off calcium, tin and uranium isotopes, as a function of the asymmetry parameter  $\delta$ . The variation of the first scattering minimum with the neutron skin of neighboring isotopes,  $\Delta q_1 \simeq 2/A^{8/3} \text{ fm}^{-1}$  is very small to be measured accurately. The first minimum changes from 220 MeV/c for  $^{35}\text{Ca}$  to 204 MeV/c for  $^{53}\text{Ca}$ , an approximate 7%, which is certainly within the experimental resolution. Of course, sudden changes of the neutron skin with  $\delta$  might happen due to shell closures and other microscopic effects and are expected to be observed in future experiments.

To be more specific, let us assume that a goal for the electron scattering experiment is to get accurate results for the charge radius  $\langle r_p^2 \rangle^{1/2}$ , so that  $\delta \langle r_p^2 \rangle^{1/2} < 0.05 \text{ fm}$ . According to the numbers obtained above, this implies that the percent measurement of the first minimum has to be  $(\Delta q_1/q_1) < q_1 [\text{fm}^{-1}] \%$ , with  $q_1$  in units of  $\text{fm}^{-1}$  and the right-hand side of the inequality yielding the percent value. For example, for  $^{53}\text{Ca}$   $q_1 = 1.11 \text{ fm}^{-1}$  meaning that the experimental resolution on the value of  $q_1$  has to be within 1% to achieve the required accuracy. The situation improves for heavier nuclei, as becomes evident from figure 2.

A second possibility to measure the dependence of the differential cross sections on the neutron skin is to look for variations of the height of the second bump, the bump after the first minimum in figure 1. This bump occurs at  $q_m \simeq 6/R_p$ . If the density closely follows the parametrization of eq. 37, then the peak of  $|F(q)|^2$  will be reduced compared to the first maximum by a factor  $[g(q_m a)/12]^2$ , where  $g(q_m a)$  is a function of the diffuseness parameter  $a$ . In the case of eq. 37  $g$  is the Fourier transform of an Yukawa function and its value at  $q_m a$  is of the order of 1/2 and its variation around  $q_m$  is weak. However, a different parametrization of the diffuseness can lead to appreciable changes in  $g(qa)$ , as can be verified by using eq. 35 which shows an exponential decrease of  $g$  with  $q$ . Thus, the dependence of the height of the second maximum of the differential cross section on the neutron skin is a less appropriate tool than a simple measurement of the first minimum. Of course, the ultimate test of a given theoretical model will be a good reproduction of the measured data, below and beyond the first minimum.

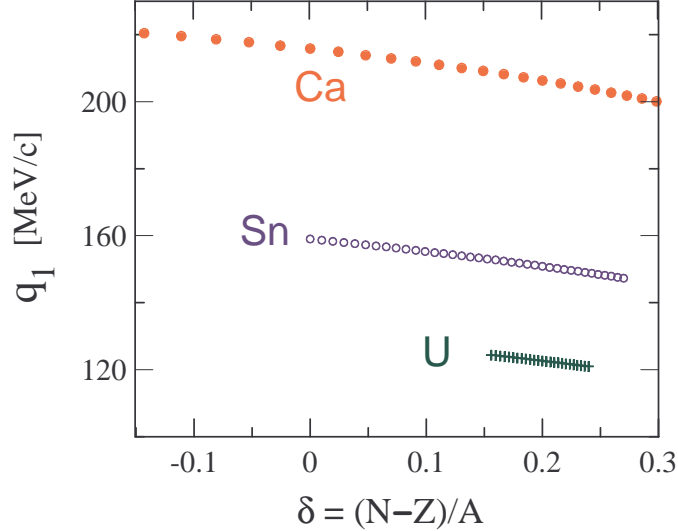


FIG. 2: Position of the first minimum  $q_1$  for elastic electron scattering off calcium, tin and uranium isotopes, as a function of the asymmetry parameter  $\delta$ .

## B. Neutron halos

For loosely bound proton-rich nuclei, elastic electron scattering will be very important to determine their charge distributions. Basic information about the charge distribution in proton-rich nuclei, e.g.  ${}^8\text{B}$  has been obtained in nucleon knockout reactions of a secondary radioactive beam interacting with a fixed target [21]. Elastic electron scattering will give more details on the distribution.

For light nuclei composed by a core nucleus and an extended distribution of halo nucleons, the form factor according to eq. 40 can expressed as

$$F(q) = (1 - g) \exp(-q^2 a_1^2/4) + \frac{g}{1 + a_2^2 q^2}, \quad (14)$$

where the density was normalized to one and in the equation above  $g$  is the fraction of nucleons in the halo. Taking  ${}^{11}\text{Li}$  as an example, the following set of parameters can be used  $g = 0.18$ ,  $a_1 = 2.0$  fm and  $a_2 = 6.5$  fm. Although only few nucleons are in the halo they change dramatically the appearance of the squared form factor, as shown in figure 3. The dashed curve is the squared form factor of the core alone and the dotted curve that of the halo nucleons. When the core and halo nucleon distributions are combined the squared form factor for the total matter distribution clearly displays the halo signature, as seen by the solid curve. Thus, even when the individual contribution of the halo nucleons is small

and barely visible in the plot of the matter distribution, it is very important for the form factor of the total matter distribution. It is responsible for the narrow peak which develops at low momentum transfers. This signature of the halo was indeed the motivation for the early experiments with radioactive beams. The narrow peak was observed in momentum distributions following knockout reactions [1].

Elastic electron scattering will not be sensitive to the narrow peak of  $|F(q)|^2$  at small momentum  $q$ , but to the form factor of the charge distribution,  $|F_{ch}(q)|^2$ , which in the case of  $^{11}\text{Li}$  will be similar to the dashed curve in figure 3. The determination of this form factor will tell us if the core has been appreciably modified due to the presence of the halo nucleons. Very likely this form factor will not be much different than that of the free core nucleus. As noted from eq. 14 and figure 3, the form factor is poor in details. It will be hard to verify if its charge distribution deviates appreciably from a Gaussian distribution. The basic information which can be extracted from the experimental data will be the width of the distribution. It is worthwhile mentioning that many of what we call core nuclei are also short-lived and very little is known about their charge distribution. This can be shown by comparing the dashed curve in figure 3 with that arising from a Hartree-Fock (HF) calculation for the charge density.

In order to explain the spin, parities, separation energies and size of exotic nuclei consistently a microscopic calculation is needed. One possibility is to resort to a HF calculation. Unfortunately, the HF theory cannot provide the predictions for the separation energies within the required accuracy of hundred keV. Here we use a simple and tractable HF method [22] to generate synthetic data for the charge-distribution in  $^{11}\text{Li}$ . Details of this method is described in ref. [23]. Assuming spherical symmetry, the Hartree-Fock equation for the Skyrme interaction can be written as

$$\left[ -\nabla \frac{\hbar^2}{2m^*(r)} \nabla + V(\mathbf{r}) \right] \psi_i(\mathbf{r}) = \epsilon_i \psi_i(\mathbf{r}) \quad (15)$$

where  $m^*(r)$  is the effective mass. The potential  $V(\mathbf{r})$  has a central, a spin-orbit and a Coulomb term

$$V(\mathbf{r}) = V_{\text{central}} + V_{\text{spin-orbit}} + V_{\text{Coulomb}}. \quad (16)$$

The central potential is multiplied by a constant factor  $f$  only for the last neutron

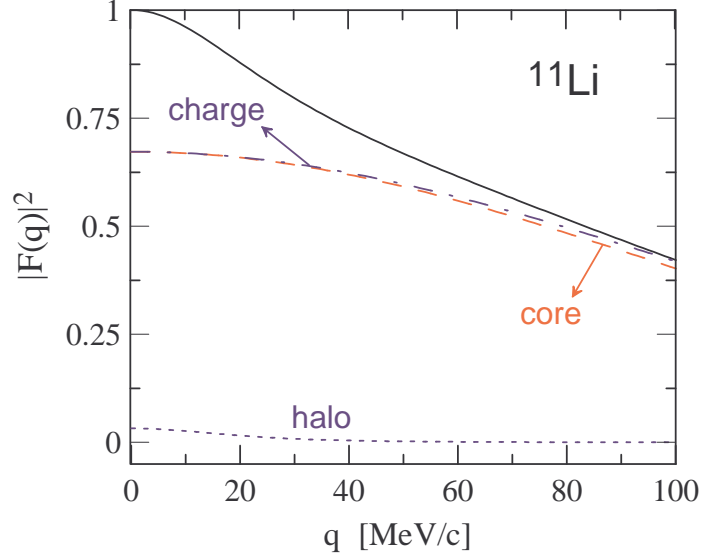


FIG. 3: Form factor squared for  $^{11}\text{Li}$  showing the individual contributions of the core and of the halo nucleons. When the core and halo nucleon distributions are taken together the squared form factor for the total matter distribution is given by the solid curve.

configuration:

$$V_{\text{central}}(r) = fV_{HF}(r), \begin{cases} f \neq 1 & \text{for last neutron configuration} \\ f = 1 & \text{otherwise.} \end{cases} \quad (17)$$

As the effective interaction, a parameter set of the density dependent Skyrme force, so called BKN interaction [24], is adopted. The parameter set of BKN interaction has the effective mass  $m^*/m = 1$  and gives realistic single particle energies near the Fermi surface in light nuclei. The original BKN force has no spin-orbit interaction. In our calculations, we introduce the spin-orbit term in the interaction so that the single-particle energy of the last neutron orbit becomes close to the experimental separation energy. In this way, the asymptotic form of the loosely-bound wave function becomes realistic in the neutron-rich nucleus. In order to obtain the nuclear sizes, the rms radii of the occupied nucleon orbits are multiplied by the shell model occupation probabilities, which are also obtained in the calculations. The large r.m.s. radii of the valence neutron orbits is attributed to the small separation energy. The calculated value is close enough to create the halo structure in the HF wave functions. In  $^{11}\text{Li}$ , the last occupied orbits is taken to be  $1p_{1/2}$  and  $2s_{1/2}$ .

We took the cut-off radius of H-F calculation to be  $R = 40$  fm which is necessary to

include properly the loosely bound nature of the neutron wave function. The separation energy for the valence nucleons is  $S_{2n}(theo) = 0.274$  MeV, which is to be compared with the experimental one  $S_{2n}(exp) = 0.30$  MeV. The column indicated by  $j_{\text{halo}}$  in Table 1 displays the most probably occupied orbits. The final radius is obtained by adding the core radius, and is given in the row indicated by SM. Of course, the factor  $f$  in Eq. 17 is arbitrary ( $f = 0.82$  for the last neutrons in  $^{11}\text{Li}$  [22]) and deserves a satisfactory explanation.

	$j_{\text{halo}}$	$\sqrt{\langle r^2 \rangle}_{\text{cal}}$ (fm)	$\sqrt{\langle r^2 \rangle}_{\text{exp}}$ (fm)
$^9\text{Li}$ (core)		2.45	$2.41 \pm 0.02$
$^{11}\text{Li}$	$1p_{1/2}$	5.36	
	$2s_{1/2}$	7.61	
SM		3.26	$3.16 \pm 0.11$

Table 1 - Single particle properties of  $^{11}\text{Li}$ . The second column gives the spins of the most probable occupied orbits. The third column is the result of Hartree-Fock calculations for the rms radii associated with these orbits, and the last column gives the rms radii of the matter distribution of these nuclei.

The elastic form factor for the matter distribution obtained in the HF calculations are very close to the ones calculated by the empirical formula 14. In figure 3 we show the charge form factor,  $|F_{ch}(q)|^2$ , by a dashed-dotted line. One sees very little difference from the simpler empirical parametrization of eq. 14. The conclusion for the  $^{11}\text{Li}$  case is that data on elastic electron scattering will hardly distinguish between simple models, as e.g. eq. 14, and more elaborate models which also reproduce the basic features of the nucleus, e.g. its root-mean-square radius. The lack of minima, and of secondary peaks (as shown in eq. 14), make it difficult to extract from  $|F_{ch}(q)|^2$  more detailed information on the charge-density profile.

It is worthwhile to mention that the deviation of the nuclear charge distribution from a simple shell-model is not peculiar of an exotic nucleus. For example, in the case of  $^6\text{Li}$  a good fit to experimental data was obtained with [25]

$$|F_c(q)|^2 = \exp(-a^2 q^2) - C \exp(-b^2 q^2),$$

with  $a = 0.933$  fm,  $b = 1.3$  fm, and  $C = 0.205$ . However, the data cannot be fitted by using a model in which the nucleons move in a single-particle potential.

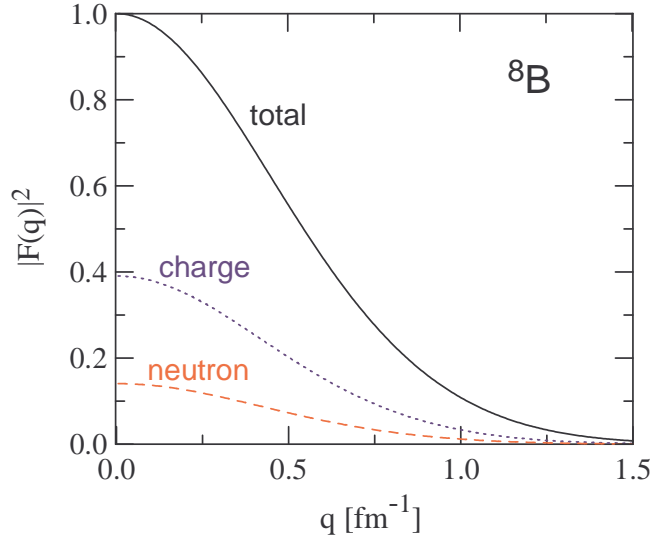


FIG. 4: Form factor squared for  ${}^8\text{B}$  showing the contribution of neutron (dashed), charge (dotted) and total (solid) matter distribution of nucleons.

### C. Proton Halos

As a prototype of proton halo nucleus, we will consider here the case of  ${}^8\text{B}$ . This nucleus perhaps is the most likely candidate for having a proton halo structure, as its last proton has a binding energy of only 137 keV. The charge density for this nucleus can be calculated in the framework of the Skyrme Hartree-Fock model. We will use here the results obtained in ref. [26], where axially symmetric Hartree-Fock equations were used with SLy4 [27] Skyrme interaction which has been constructed by fitting to the experimental data on radii and binding energies of symmetric and neutron-rich nuclei. In their calculations pairing correlations among nucleons have been treated within the BCS pairing method. The form factor squared for the charge density in  ${}^8\text{B}$  is shown in figure 4.

The signature for a proton halo would be the small width of the charge distribution, as compared to the neutron, or the total matter distribution. The width of the charge form factor squared corresponding to the plot in figure 4 is  $\Delta_{ch} = 0.505 \text{ fm}^{-1} = 99.6 \text{ MeV}/c$ . The corresponding values for the neutron and the total matter distributions are, respectively,  $\Delta_n = 0.512 \text{ fm}^{-1} = 101 \text{ MeV}/c$  and  $\Delta_{tot} = 0.545 \text{ fm}^{-1} = 108 \text{ MeV}/c$ . This amounts to approximately 10% differences of matter and charge form factors,  $|F_{ch}(q)|^2$ , in  ${}^8\text{B}$ .

The proton halo in  ${}^8\text{B}$  is mainly caused by the loosely-bound extra proton in the  $p_{3/2}$

orbit. It is thus important to know how much of the charge form factor seen in figure 4 arises from this extra-proton. Let us assume a single-particle model for simplicity. It is clear that for such a narrow halo (or skin?) the size of the nucleon also matters. The relevance of the nucleon size is shown in figure 5 where a slice of the nucleon is included in a thin spherical shell of radius  $r$  and thickness  $dr$  from the center of the nucleus. If the position of the nucleon is given by  $R$ , the part of the proton charge included in the spherical shell is given by

$$d\rho_{ch} = 2\pi r^2 dr \int_0^\pi d\theta \rho_p(\mathbf{x}) \sin\theta, \quad (18)$$

where  $\rho_p(\mathbf{x})$  is the charge distribution inside a proton at a distance  $\mathbf{x}$  from its center. The coordinates are shown in figure 5. They are related by  $x^2 = r^2 + R^2 - 2rR \cos\theta$ . The contribution to the nuclear charge distribution from a single-proton in this spherical shell is thus given by  $\mathcal{N}_p(R, r) = d\rho_{ch}/4\pi r^2 dr$ .

Assuming that the charge distribution of the proton is described either by a Gaussian or a Yukawa form (see Appendix), the integral in eq. 18 can be performed analytically, yielding

$$\mathcal{N}_p^{(G)}(R, r) = \frac{1}{4\pi^{1/2}arR} \begin{cases} \frac{1}{\pi} \left\{ \exp\left[-\frac{(R-r)^2}{a^2}\right] - \exp\left[-\frac{(R+r)^2}{a^2}\right] \right\}, & \text{for a Gaussian dist.} \\ \frac{1}{2} \left\{ \exp\left[-\frac{|R-r|}{a}\right] - \exp\left[-\frac{|R+r|}{a}\right] \right\}, & \text{for a Yukawa dist.,} \end{cases} \quad (19)$$

where  $a$  is the proton radius parameter.

The charge distribution at the surface of a heavy proton-rich nucleus,  $\delta\rho_{ch}(r)$ , may be described as a pile-up of protons forming a skin. Let  $n_i$  be the number of nucleons in the skin and  $R_i$  be the distance of these protons to the center of the nucleus. One gets

$$\delta\rho_{ch}(r) = \sum_i n_i \mathcal{N}_p(r, R_i). \quad (20)$$

Assuming  $R_i$  to be constant, equal to the nuclear charge radius  $R$ , and using eqs. 19 it is evident that while the density at the surface increases, its size  $R$  and width  $a$ , remain unaltered. The form factor associated with this charge distribution is given by

$$\delta F_{ch}(q) = \frac{4\pi}{q} \sum_i n_i \int_0^\infty dr r \mathcal{N}_p(r, R_i) \sin(qr) = \exp(-qa^2) \sum_i n_i \frac{\sin(qR_i)}{qR_i}, \quad (21)$$

where the last result is for the Gaussian distribution in eq. 19. An analytical expression can also be obtained for the Yukawa distribution. For  $R_i = R$ , expression 21 shows that the increase of density in the skin does not change the shape of the form factor, or of the

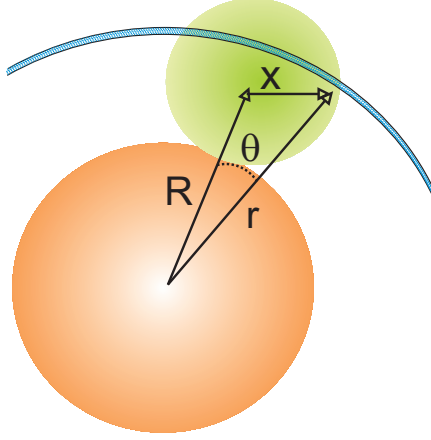


FIG. 5: An spherical shell with radius  $r$  from the center of the nucleus will have a charge contribution from inside a nucleon located at a distance  $R$ .

cross section, but just its normalization. The fall down of the cross section is determined by  $a$  alone, and not by  $n_i$ . If the charge of additional protons is distributed homogeneously across the nucleus including the skin, the normalized form factor will not change, except for a small change in  $R$ .

For a proton halo nucleus it is more appropriate to change  $\sum_i n_i \rightarrow 4\pi \int dR R^2 \mathcal{N}_p(r, R) \delta\rho_{ch}(R)$ , where  $\delta\rho_{ch}(R)$  is the density change created by the extended wavefunction of the halo protons. We then recast eq. 21 in the form

$$\delta F_{ch}(q) = \frac{4\pi}{q} \exp(-qa^2) \int_0^\infty dR R \delta\rho_{ch}(R) \sin(qR). \quad (22)$$

The shape of the form factor is here dependent not only on the proton size but also on the details of the halo density distribution. To assess this information let us consider the  $^8\text{B}$  case again. In this case, the halo size is determined by the valence proton in a  $p_{3/2}$  orbit. The density  $\delta\rho_{ch}(R)$  due this proton can be calculated with a simple Woods-Saxon model. Using the same potential parameters as given in ref. [28] we show in fig. 6 the form factor  $|\delta F_{ch}(q)|^2$  compared to the charge form factor  $|F_{ch}(q)|^2$  of figure 4. It is evident that the halo contributes to a narrow form factor. However, in contrast to the neutron halo case shown in figure 3, the charge form factor of  $^8\text{B}$  does not show a pronounced influence of the halo charge distribution.

The low energy expansion of the form factor, eq. 3, allows the extraction of the rms

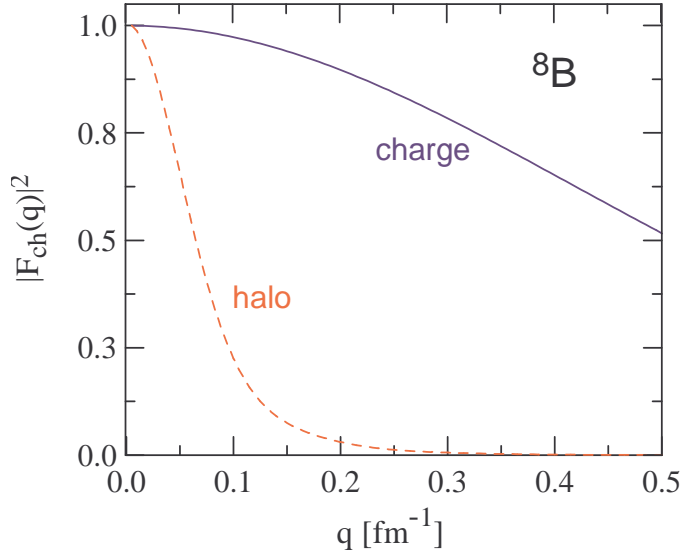


FIG. 6: The charge form factor squared of  ${}^8\text{B}$  (solid line). Also shown is the charge form factor squared due only to the valence halo proton.

radius of the charge distribution from

$$\langle r_{ch}^2 \rangle = -6 \left[ \frac{dF_{ch}}{d(q^2)} \right]_{q^2=0}. \quad (23)$$

Applying this relationship to the charge form factor used in figure 6 we get  $\langle r_{ch}^2 \rangle^{1/2} = 2.82$  fm which is close to the experimental value  $\langle r_{ch}^2 \rangle_{\text{exp}}^{1/2} = 2.76 \pm 0.08$  fm. The shape of the charge form factor is also well described by a Gaussian distribution (see Appendix) with radius parameter  $a = 2.30$  fm. In contrast to the case of  ${}^{11}\text{Li}$  as seen in figure 3, the proton halo in  ${}^8\text{B}$  does not seem to build up a two-Gaussian shaped form factor. This observation also seems to be compatible with the momentum distributions of  ${}^7\text{Be}$  fragments in knockout reactions using  ${}^8\text{B}$  projectiles in high energy collisions [21]. Electron scattering experiments will help to further understand this property of proton halos.

#### IV. INVERSE SCATTERING PROBLEM

In PWBA the inverse scattering problem can be easily solved. It is possible to extract the form factor from the cross section and then, with an inversion of the Fourier transform,

to get the charge density distribution

$$\rho_{ch}(r) = \frac{1}{2\pi^2} \int_0^\infty dr q^2 j_0(qr) F_{ch}(q). \quad (24)$$

As we discussed in previous sections, the PWBA approximation can be justified only for light nuclei (e.g.  $^{12}\text{C}$ ) in the region far from the diffraction zeros. For higher  $Z$  values the agreement with experiment is only of a qualitative nature.

It is very common in the literature to use a theoretical model for  $\rho_{ch}(r)$ , e.g. the Hartree-Fock calculations discussed in the previous sections and compare to the cross section experimental data. When the fit is “reasonable” (usually guided by the eye) the model is considered a good one. However, whereas the theoretical  $\rho_{ch}(r)$  can contain useful information about the central part of the density (e.g. bubble-like nuclei, with a depressed central density), an excellent fit to the available experimental data does not necessarily mean that the data is sensitive to those details. The obvious reason is that short distances are probed by larger values of  $q$ . Experimental data from electron-ion colliders will suffer from limited accuracy at large values of  $q$ , possibly beyond  $q = 1 \text{ fm}^{-1}$ . Thus it is useful to identify what are the conditions for reproducing as well as possible the nuclear density within a theory independent fit.

In order to obtain an unbiased “experimental”  $\rho_{ch}(r)$  one usually assumes that the density is expanded as

$$\rho_{ch}(r) = \sum_{n=1}^{\infty} a_n f_n(r), \quad (25)$$

where the basis functions  $f_n(r)$  are drawn from any convenient complete set and the expansion coefficients  $a_n$  are fixed to reproduce the differential elastic cross section. The corresponding Fourier transform then takes the form

$$\tilde{\rho}(q) \equiv F_{ch}(q) = \sum_{n=1}^{\infty} a_n \tilde{f}_n(q), \quad (26)$$

where

$$\tilde{f}_n(q) = 4\pi \int_0^\infty dr r^2 j_0(qr) f_n(r). \quad (27)$$

represents basis functions in momentum space.

Evidently the sum in eq. 25 has to be truncated and this produces an error in the determination of the charge density distribution. Another problem is that, as shown by eq. 24, the solution of the inverse scattering problem requires an accurate determination

of the cross section up to large momentum transfers. Electron scattering experiments in electron-ion colliders will be performed within a limited range of  $q$  and this will produce an uncertainty in the determination of the charge density distribution. As we have discussed in previous sections, the measurements have to encompass the first few minima of the cross section for heavy nuclei in order that the density profile can be mapped. In the case of proton halos, measurements at large  $q$  might not be so critical, as we have seen for the case of  $^8\text{B}$  discussed in the previous section.

We consider two bases that have been found useful [29] in the analysis of electron or proton scattering data. The present discussion is limited to spherical nuclei, but generalizations to deformed nuclei can be done.

The Fourier-Bessel (FB) expansion (i.e. with  $f_n$  taken as spherical Bessel functions) is useful because of the orthogonality relation between spherical Bessel functions

$$\int_0^{R_{\max}} dr r^2 j_l(q_n r) j_l(q_m r) = \frac{1}{2} R_c^3 [j_{l+1}(q_n R_{\max})]^2 \delta_{nm}, \quad (28)$$

where the  $q_n$  are defined such as

$$j_l(q_n R_{\max}) = 0. \quad (29)$$

The FB basis implies that the charge density  $\rho_{ch}(r)$  should be zero for values of  $r$  larger than  $R_{\max}$ . For example, the basis can be defined as follows

$$\begin{aligned} f_n(r) &= j_0(q_n r) \Theta(R_{\max} - r), \\ \tilde{f}_n(q) &= \frac{4\pi (-1)^n R_{\max}}{q^2 - q_n^2} j_0(q R_{\max}), \end{aligned} \quad (30)$$

where  $\Theta$  is the step function,  $R_{\max}$  is the expansion radius and  $q_n = n\pi/R_{\max}$ .

In principle it is possible to obtain the  $a_n$  coefficients measuring directly the cross section at the  $q_n$  momentum transfer. If the form factor (2) is known at  $q_n$ , the coefficients  $a_n$  can be obtained inserting (28) and (30) in the definition (2) of the form factor, leading to

$$a_n = \frac{F_{ch}(q_n)}{2\pi R_{\max}^3 [j_1(q_n R_{\max})]^2}. \quad (31)$$

In general the cross sections are measured at  $q$  values different from  $q_n$ . Using the expansion (30) of the charge density we find for the form factor the relation

$$F_{ch}(q) = \frac{4\pi}{q} \sum_n a_n \frac{(-1)^n}{q^2 - q_n^2} \sin(q R_{\max}). \quad (32)$$

By fitting the experimental  $F_{ch}(q)$  one obtains the  $a_n$  parameters and reconstruct the nuclear charge density. Analysis of this type are often described as model independent because a complete basis can reproduce any physically reasonable density; if a sufficient number of terms are included in the fitting procedure the dependence of the fitted density upon the assumptions of the model is minimized. By contrast, simple parametrizations like the ones described in the Appendix severely constrain the shape of the fitted density.

Note that not all  $a_n$ 's are needed. Since the integral of the density, or  $F(q=0)$ , is fixed to the charge number (or normalized to the unit) there is one less degree of freedom. Also, densities tend to zero at large  $r$ . Thus another condition can be used, e.g. that the derivative of the density is zero at  $R_{\max}$ . Thus, when we talk about  $n$  expansion coefficients we mean in fact that only  $n-2$  coefficients need to be used in eq. 32.

As seen above, one advantage of the FB expansion is that the contribution of each term to the form factor is concentrated around its characteristic frequency  $q_n$  so that a coefficient  $a_n$  is largely determined by data with  $q \sim q_n$ . The larger the expansion radius  $R_{\max}$ , the smaller the spacing between successive  $q_n$  and the greater the sensitivity one has to variations in the form factor (eq. 31). One should choose  $R_{\max}$  to be several times the rms charge radius but not so large that an excessive number of terms is needed to span the experimental range of momentum transfer. Terms with  $q_n > q_{\max}$  provide an estimate of the incompleteness error. But the results are insensitive to the exact value of  $R_{\max}$  as long as the appropriate number of terms are included in eq. 32. For experiments performed up to  $q_{\max}$  the number of expansion coefficients needed for the fit is determined by  $n_{\max} \simeq q_{\max} R_{\max} / \pi$ .

A disadvantage of the FB expansion is that a relatively large number of terms is often needed to accurately represent a typical confined density, e.g. for light nuclei. One can use other expansion functions which invoke less number of expansion parameters, e.g. the Laguerre-Gauss (LG) expansion,

$$f_n(r) = e^{-\alpha^2} L_n^{1/2}(2\alpha^2), \quad \text{and} \quad \tilde{f}_n(q) = 4\pi^{3/2}\beta^3 (-1)^n e^{-\gamma^2} L_n^{1/2}(2\gamma^2),$$

where  $\alpha = r/\beta$ ,  $\gamma = q\beta/2$ , and  $L_n^p$  is the generalized Laguerre polynomial. Another possibility is to use an expansion on Hermite (H) polynomials. In both cases, the number of terms needed to provide a reasonable approximation to the density can be minimized by choosing  $\beta$  in accordance with the natural radial scale. For light nuclei  $\beta = 1 - 2$  fm can be chosen, consistent with the parametrization of their densities. Then the magnitude of  $a_n$

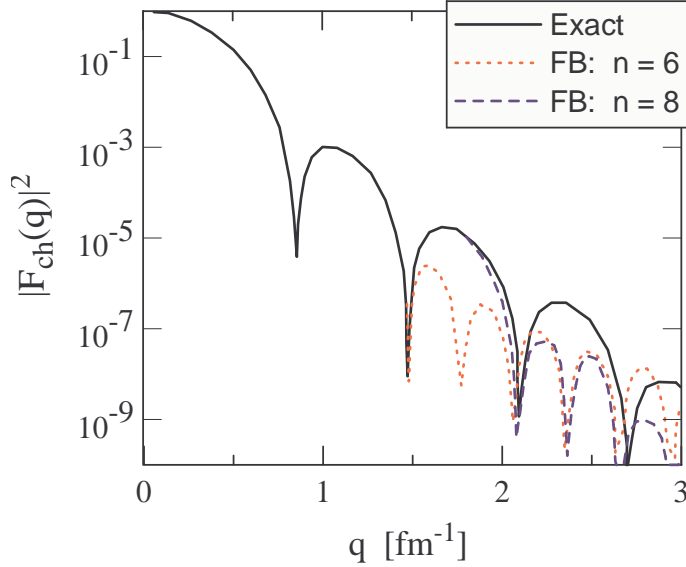


FIG. 7: Form factor squared for a Fermi function charge distribution with half-density radius  $R = 5.2$  fm and diffuseness  $a = 1.2$  fm (solid line). The dotted line is obtained with the FB expansion, eq. 32, up to  $n = 6$ . The dashed curve uses up to  $n = 8$ .

decreases rapidly with  $n$ , but the quality of the fit and the shape of the density are actually independent of  $\beta$  over a wide range. The disadvantage of the LG of H expansions is that the basis functions are not localized in momentum space so that the coefficients tend to be correlated more strongly than for the FB expansion. As shown by application to a few cases, the main information on skin and halo sizes can be obtained using the FB expansion without problems.

Figure 7 shows the charge form factor squared for a Fermi function distribution with half-density radius  $R = 5.2$  fm and diffuseness  $a = 1.2$  fm (solid line). The dotted line is obtained with the FB expansion, eq. 32, up to  $n = 6$ . The dashed curve uses up to  $n = 8$ . One clearly sees that the latter improves the fit to the form factor up to the third minimum in passing from  $n = 6$  to the expansion with  $n = 8$ . We use  $R_{\max} = 15$  fm, so that adding the  $n = 8$  term improves the fit of the distribution including the peak at  $q \simeq 1.75$  fm $^{-1}$ , as seen in the figure.

For real data, the expansion coefficients  $a_n$  are obtained by minimizing

$$\chi^2 = \sum_i \left( \frac{y_i - y(q_i, a_n)}{\sigma_i} \right)^2,$$

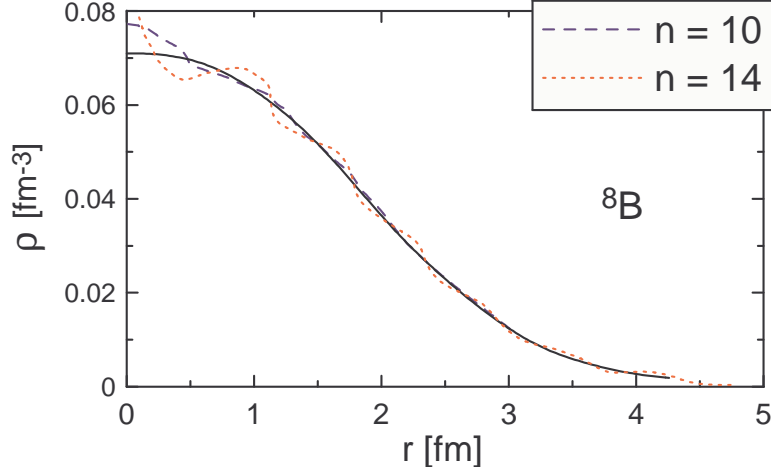


FIG. 8: Hartree-Fock charge density of  ${}^8\text{B}$  (solid line). The dashed and dotted lines are the solution of the inverse scattering problem using a Fourier-Bessel expansion with  $n = 10$  and  $n = 14$  terms, respectively.

where  $y(q_i, a_n)$  is the fitted value of the cross section (form factor) with a set of coefficients  $a_n$  and  $y_i$  are the experimental data at momentum  $q_i$  with uncertainty  $\sigma_i$ .

To check the limitations of this procedure, we generate a set of pseudodata for  ${}^8\text{B}$ . The calculated charge form factor of figures 4 and 6 is used to generate 40 data points equally spaced by  $\Delta q = 0.02 \text{ fm}^{-1}$ . These data were given an uncertainty  $\sigma_i$  linearly increasing with  $q_i$ , from 1% for  $q_i = 0.02 \text{ fm}^{-1}$  to 20% for  $q_i = 0.82 \text{ fm}^{-1}$ .

The best fit, with  $R_{\text{max}} = 10 \text{ fm}$ , is obtained with  $n = 10$  expansion coefficients. Increasing the number of coefficients does not improve the quality of the fit, as is shown in figure 8 for  $n = 14$ . It only produces more oscillations of the density. The reason is that terms with larger  $n$ 's are only needed to reproduce the data at larger values of momentum transfer, as shown in fig. 7. The fit to the data for  $q < q_{\text{max}}$  is not affected but the presence of these new terms introduces oscillations in the charge distribution. A possible fix to this problem is to include pseudodata in addition to experimental data. This method is well known in the literature [29]. The pseudodata are used to enforce constraints and to estimate the incompleteness error associated with the limitation of experimental data to a finite range of momentum transfer.

## V. CONCLUSIONS

In this work we studied the electron scattering off unstable nuclei. This work is complementary to previous works in this direction (see e.g. ref. [10]). Particular attention was given to the effect of the neutron (proton) skin on the scattering form factors. It was shown that the position of the first minimum is arguably the best signature to look for noticeable changes in the charge radius size.

The evidence for a proton halo is not so clear as in the case of other probes. For example, it is well known that  ${}^7\text{Be}$  fragments arising from the proton knockout of  ${}^8\text{B}$  projectiles display a distinctively narrow momentum distribution characteristic of a long tail of the valence proton in  ${}^8\text{B}$  [21]. This feature is a consequence of the peripheral character of the knockout process, which is ideal to probe the tail of the bound states. Nonetheless, due to the Coulomb barrier the bulk of the charge in the nucleus is confined close to its center. Electron scattering is sensitive to this bulk charge and therefore does not display such a strong halo signature.

The minimum information obtained with electron scattering in electron-ion colliders will be the rms charge radius,  $\langle r_{ch}^2 \rangle^{1/2}$ . This information “per se” is very valuable. It is sensitive to the skin size in a heavy nucleus. But it also depends on the accuracy with which this quantity can be measured. As we have shown in the previous sections, it will be necessary to go beyond the first minimum to extract information about the central value of the charge density. It might also be necessary to have some theoretical guidance to include pseudo-data in the experimental analysis in order to obtain a better information about the central charge densities.

## VI. APPENDIX 1 - ANALYTICAL FORM FACTORS

Here we summarize the analytical expressions for the charge form factors which are used in this work, for guidance purpose. One example of analytical parametrization of the nuclear charge density is given by the hard sphere (uniform distribution with sharp cutoff at  $R$ )

$$\rho(r) = \begin{cases} \rho_0 & \text{for } r \leq R \\ 0, & \text{otherwise.} \end{cases} \quad (33)$$

The form factor for this distribution is

$$F(q) = \frac{4\pi\rho_0}{q^3} [\sin(qR) - qR \cos(qR)]. \quad (34)$$

For an Yukawa distribution of the form  $\rho(r) = \rho_0 e^{-r/a}(a/r)$  one gets

$$F(q) = \frac{4\pi\rho_0 a^3}{1 + a^2 q^2}.$$

Another common parametrization is the symmetrized Fermi distribution [31]

$$\rho(r) = \rho_0 \frac{\cosh(R/a)}{\cosh(R/a) + \cosh(r/a)}.$$

For this density an analytical expression of the form factor can be easily obtained [32]:

$$F(q) = -\frac{4\pi^2\rho_0 a \cosh(R/a)}{q \sinh(R/a)} \left[ \frac{R \cos(qR)}{\sinh(\pi qa)} - \frac{\pi d \sin(qR) \cosh(\pi qa)}{\sinh^2(\pi qa)} \right].$$

The above expression is composed of oscillating terms damped by exponentials. This is better seen taking the limit for  $qa \gg 1$ . We obtain:

$$F(q) \simeq -\frac{4\pi^2\rho_0 a}{q} [R \cos(qR) - \pi a \sin(qR)] e^{-\pi qa}, \quad (35)$$

where the oscillating and damping terms are evident.

The Fermi distribution

$$\rho(r) = \rho_0 / [1 + \exp \{(r - R) / a\}] \quad (36)$$

with central density  $\rho_0$ , radius  $R$ , and diffusiveness  $a$ , gives a good description of the densities of heavy nuclei. This distribution is also well described by the convolution  $\rho(\mathbf{r}) = \int d^3r' \rho_p(\mathbf{r}) \rho_A(\mathbf{r} - \mathbf{r}')$  of a hard sphere for  $\rho_A(\mathbf{r} - \mathbf{r}')$  and an Yukawa function [30] for  $\rho_p(\mathbf{r})$ . In this case,  $F(q) = F_p(q)F_A(q)$ , can be calculated analytically as

$$F(q) = \frac{4\pi\rho_0}{q^3} [\sin(qR) - qR \cos(qR)] \left[ \frac{1}{1 + q^2 a_Y^2} \right]. \quad (37)$$

The term inside the first parenthesis comes from the hard sphere (uniform distribution with sharp cutoff at  $R$ ) and the second parenthesis is the damping term due to an Yukawa diffuseness surface with width  $a_Y$ .

Figure 9 compares  $F(q)$  of eq. 37 obtained with the numerical integration of a two-point Fermi density distribution, eq. 36. The parameters for Al ( $R = 3.07$  fm ,  $a = 0.519$  fm), Cu ( $R = 4.163$  fm ,  $a = 0.606$  fm), Sn ( $R = 5.412$  fm ,  $a = 0.560$  fm), Au ( $R = 6.43$  fm ,  $a = 0$ .

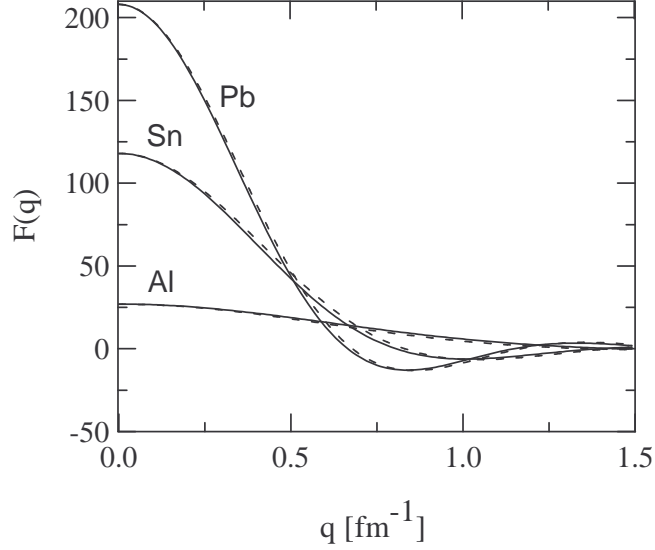


FIG. 9: Comparison between form factors of a convoluted Fermi-Yukawa distribution calculated numerically using eq. 36 (solid lines), or with the analytical equation 37 (dashed lines).

541 fm) , and Pb ( $R = 6.62$  fm ,  $a = 0.546$  fm) (to simplify the figure, we did not plot the curves for Au and Cu). In all cases we used for the Yukawa function parameter in eq. (37)  $a_Y = 0.7$  fm. We see that the agreement is very good.

For light nuclei, it is more appropriated to use a Gaussian density, with the Gaussian parameter  $a = \sqrt{\frac{2}{3} \langle r^2 \rangle_{ch}}$ , where  $\sqrt{\langle r^2 \rangle_{ch}}$  is the root-mean-square radius of the matter density. For example, for carbon,  $a = 2.018$  fm. For a Gaussian density parametrized as  $\rho(r) = \rho_0 \exp(-r^2/a^2)$ , one gets

$$F(q) = (\pi a^2)^{3/2} \rho_0 \exp(-q^2 a^2/4) . \quad (38)$$

To simulate nodes in the wavefunctions of light nuclei, a sum of gaussian distributions can be used, including terms proportional to  $r^n \exp(-r^2/a^2)$ . The form factors arising from these terms can be obtained from nth-order derivatives of eq. 38 with respect to  $1/a^2$ .

For halo nuclei the following parametrization can be adopted

$$\rho(r) = \rho_1 \exp(-r^2/a_1^2) + \rho_2 \left(\frac{a_2}{r}\right) \exp(-r/a_2) , \quad (39)$$

where the first term describes the density of the core and the second term describes the extended halo density. If the core contains  $A_1$  nucleons and the halo contains  $A_2$  nucleons,

the form factor for the above distribution becomes

$$F(q) = A_1 \exp(-q^2 a_1^2/4) + \frac{A_2}{1 + a_2^2 q^2}. \quad (40)$$

### Acknowledgments

The author is grateful to Haik Simon for beneficial discussions.

- 
- [1] I. Tanihata et al., Phys. Rev. Lett. **55** (1985) 2676.
  - [2] C.A. Bertulani, M.S. Hussein, and G. Münzenberg, *Physics of Radioactive Beams* (Nova Science Publishers, Hauppauge, NY, 2002).
  - [3] A. Ozawa, T. Suzuki and I. Tanihata, Nucl. Phys. **A693** (2001) 32.
  - [4] R. Hofstadter, Nobel Lectures, available at <http://nobelprize.org/physics/laureates/1961/hofstadter-lecture.p>
  - [5] *Technical Proposal for the Design, Construction, Commissioning, and Operation of the ELISE setup*, spokesperson Haik Simon, GSI Internal Report, Dec. 2005.
  - [6] T. Suda, K. Maruyama, *Proposal for the RIKEN beam factory*, RIKEN, 2001; M. Wakasugia, T. Suda, Y. Yano, Nucl. Inst. Meth. Phys. A 532, 216 (2004)
  - [7] R. Hofstadter, Rev. Mod. Phys. 28, 214 (1956).
  - [8] F. Hofmann and H. Lenske, Phys. Rev. **C57**, 2281 (1998).
  - [9] S. Mizutori et al., Phys. Rev. **C61**, 0443261 (2000).
  - [10] A.N. Antonov et al., Phys. Rev. **C72**, 044307 (2005).
  - [11] R.F. Frosch et al., Phys. Rev. **174**, 1380 (1968).
  - [12] S. Galster et al., Nucl. Phys. **B32**(1971) 221 .
  - [13] W.A. McKinley and H. Feshbach, Phys. Rev. **74**, 1759 (1948).
  - [14] D.R. Yennie, D.G. Ravenhall, and R.R. Wilson, Phys. Rev. **92**, 1325 (1953); Phys. Rev. **95**, 500 (1954).
  - [15] L.S. Cutler, Phys. Rev. **157**, 885 (1967).
  - [16] J.M. Eisenberg and W. Greiner, “Excitation Mechanisms of the Nucleus”, (North-Holland, Amsterdam, 1988).
  - [17] J. Dobaczewski, W. Nazarewicz, and T. R. Werner, Z. Phys. A **354**, 27 (1996).
  - [18] P. Danielewicz, Nucl. Phys. A **727** (2003) 233.

- [19] A.W. Steiner et al., Phys. Rep. **411** (2005) 325.
- [20] A. Trzcinska et al., Phys. Rev. Lett. **87**, 082501 (2001).
- [21] W. Schwab et al., Z. Phys. **A350**, 283 (1995).
- [22] G.F. Bertsch, A.B. Brown and H. Sagawa, Phys. Rev. **C39**, 1154 (1989).
- [23] H. Sagawa and C.A. Bertulani, Prog. Theo. Phys. Suppl. **124**, 143 (1996).
- [24] P. Bonche, S. Koonin and J. W. Negele, Phys. Rev. **C13** (1976) 1226.
- [25] L.R. Suelzle, M.R. Yearian, and H. Crannel, Phys. Rev. **162**, 992 (1967).
- [26] S.S. Chandel, S.K. Dhiman and R. Shyam, Phys. Rev. **C68**, 054320 (2003).
- [27] E. Chabanat, P. Bonche, P. Haensel, J. Meyey and R. Schaeffer, Nucl. Phys. **A627** (1997) 710.
- [28] P. Navratil, C.A. Bertulani and E. Caurier, Phys. Lett. **B634** (2006) 191.
- [29] J. L. Friar and J. W. Negele, Nucl. Phys. **A212** (1973) 93.
- [30] K.T.R. Davies and J.R. Nix, Phys. Rev. **C14**, 1977 (1976).
- [31] M.E. Grypeos, G.A. Lalazissis, S.E. Massen and C.E Panos, J. Phys. G **17** (1991) 1093.
- [32] R.E. Kozak, Am. J. Phys. **59**, 74 (1991).